Mar Biol (2015) 162:1939–1954
DOI 10.1007/s00227-015-2713-x

ORIGINAL PAPER

Zooplankton in flowing water near benthic communities encounter rapidly fluctuating velocity gradients and accelerations

Rachel E. Pepper[1] · Jules S. Jaffe[2] · Evan Variano[3] · M. A. R. Koehl[4]

Received: 28 May 2014 / Accepted: 24 July 2015 / Published online: 24 September 2015

Abstract The fine-scale temporal patterns of water velocities, accelerations, and velocity gradients encountered by individual zooplankters carried in ambient flow can affect their dispersal, behavior, and interaction with other organisms, but have not yet been measured in realistic flow environments. We focused on zooplankton in wavy turbulent boundary layer flow near benthic communities because such flow affects important processes, including larval settlement and prey capture by benthic zooplanktivores. Flow across fouling communities measured in the field was mimicked in a wave flume, where time-varying velocity fields over biofouled surfaces were quantified using particle image velocimetry (PIV). Trajectories of simulated zooplankters seeded into these flow fields were followed to quantify temporal patterns of velocity gradients and accelerations that individuals encountered. We found that such zooplankters are not subjected to steady velocities or velocity gradients, but rather encounter rapidly fluctuating accelerations and velocity gradients with peaks reaching several orders of magnitude above mean values and lasting fractions of a second, much shorter than the wave period. We calculated the proportion of time zooplankters spent affected (e.g., being damaged, changing behavior) by accelerations or velocity gradients and found that a small increase in mean velocity can cause a much larger increase in time affected. Animal reaction threshold and reaction time also changed the fraction of time they were affected by the flow. Using different PIV spatial resolutions showed that inter-vector spacing should be $\leq$0.5 Kolmogorov length (smallest eddy scale) to accurately capture velocity gradients along trajectories, but coarser resolutions ($\leq$2–6 $\times$ Kolmogorov length) are sufficient for velocities, accelerations, and zooplankton trajectories.

Responsible Editor: X. Irigoyen.

Reviewed by T. Kiørboe and an undisclosed expert.

Electronic supplementary material The online version of this article (doi:10.1007/s00227-015-2713-x) contains supplementary material, which is available to authorized users.

✉ Rachel E. Pepper
rpepper77@gmail.com; rpepper@pugetsound.edu

[1] Department of Physics, University of Puget Sound, Tacoma, WA, USA

[2] Scripps Institution of Oceanography, University of California San Diego, La Jolla, CA, USA

[3] Department of Civil and Environmental Engineering, University of California Berkeley, Berkeley, CA, USA

[4] Department of Integrative Biology, University of California Berkeley, Berkeley, CA, USA

Introduction

Microscopic planktonic organisms are critical components of marine ecosystems. Their dispersal in aquatic environments, and their interactions with each other as well as with nektonic and benthic organisms are affected by the motion of the water in which they are carried. The fine-scale water flow in the immediate neighborhood of a plankter can affect processes such as nutrient or oxygen uptake (Thomas and Gibson 1990; Karp-Boss and Jumars 1998), feeding, and mating (Peters and Marrasé 2000), can interact with swimming to determine the net trajectory of a locomoting organism (Karp-Boss et al. 2000; Grunbaum and Strathmann 2003; Koehl et al. 2007; Clay and Grünbaum 2011; McDonald 2012), and may even inflict physical damage (Thomas and Gibson 1990). Flow near microscopic organisms can also elicit behavioral responses. For instance,

some species of marine larvae actively react to flow signals by altering their swimming behavior (Crisp 1955; Jonsson et al. 1991; Abelson and Denny 1997; Fuchs et al. 2013, 2015; Wheeler et al. 2015) or increasing their developmental rate (Gaylord et al. 2013).

The water flow that carries planktonic organisms in the ocean is turbulent, so velocity measured at a single location changes rapidly and stochastically in time, and the velocity of neighboring parcels of fluid is different. Since a microscopic planktonic organism is carried *with* the water around it, it does not feel local water velocity, but instead might sense the acceleration of its body as the water carrying it accelerates, and might experience local velocity gradients in space sensed as rotations, shears, stretches, or compressions. To determine the temporal patterns of water motion that planktonic organisms experience, we must approach ocean flows from a Lagrangian (measured moving with the local fluid velocity) rather than Eulerian (measured at a single point) perspective. A Lagrangian approach has been used to elucidate the temporal patterns of chemical cue concentrations encountered by microscopic marine larvae swimming in turbulent wave-driven flow over a coral reef (Koehl et al. 2007) and in gentle flow across early-stage fouling communities (Koehl and Cooper 2015). A Lagrangian approach has also been used in recent studies conducted in tanks in which idealized turbulence and waves were produced and larvae were tracked to measure water velocities, accelerations, and velocity gradients near them (Wheeler et al. 2013, 2015; Fuchs et al. 2013, 2015). However, to our knowledge, no such Lagrangian study has been done to compare the temporal patterns of velocity gradients and accelerations that zooplankton experience under different flow conditions that they experience in natural habitats. Studies of mechanical signals in idealized homogeneous isotropic turbulence in a Lagrangian framework (reviewed by Yeung 2002; Toschi and Bodenschatz 2009) have revealed that the probability density functions (PDFs) of both velocity gradients and accelerations measured in a Lagrangian framework have large tails, so fluid particles experience extreme events more often than in nonturbulent flows (Toschi and Bodenschatz 2009). These studies were done in idealized isotropic homogenous flow and thus do not allow prediction of the temporal patterns of mechanical signals encountered by organisms traveling in more complicated real-world water flow.

Most of the laboratory studies (cited above) of how microscopic planktonic organisms interact with the flow environment have also been done in idealized flow (i.e., grid-stirred turbulence, simple steady shear flow, idealized waves, or unidirectional flow). Therefore, in this study, we focus on more realistic ocean flows to determine the fine-scale fluctuations in accelerations and velocity gradients encountered by individual planktonic organisms. Understanding these fluctuations will allow for a deeper understanding of the flow plankters experience, the design of laboratory flows that accurately capture such temporal patterns, and the development of mathematical models of the consequences of plankton behavior in flow. We have focused on benthic boundary layer flow, which affects many important ecological processes, including mass exchange between the water column and the benthos, recruitment of microorganisms and invertebrate larvae into benthic communities, and prey capture by suspension feeders (Nowell and Jumars 1984). In benthic boundary layers across rough substrata in the ocean, flows are not isotropic or homogeneous, and in shallow habitats, the orbital water motion in waves further complicates the flow.

PIV resolution

A powerful technique for measuring the details of how turbulent flow fields change with time is particle image velocimetry (PIV): video records of marker particles in flowing fluid are taken, and the spatial patterns of pixel brightness in successive frames of the video are used to calculate a map of velocity vectors for each successive pair of frames (details in, e.g., Raffel et al. 1998). When using PIV to study the complex flow fields through which organisms move, there is a trade-off between making the field of view big enough to see large structures in the flow and to follow modeled plankters as they traverse realistic habitat features, versus making adjacent vectors in the flow field close enough in space to resolve accurately the velocity and its spatial gradient. Therefore, it is important to determine the PIV resolution necessary to accurately measure velocity gradients on the scale of a microscopic organism.

A theoretical estimate of the minimum spatial resolution necessary for accurate measurements of velocities and velocity gradients in turbulent flow is the Kolmogorov scale (η, the scale below which viscosity becomes the dominant sink of kinetic energy). The Kolmogorov scale is often thought of as the scale of the smallest eddies in turbulence and is typically ~56 μm to ~2 mm in the ocean (Thorpe 2007). Below the Kolmogorov scale, velocity varies smoothly and approximately linearly in space, so velocities and their spatial gradients should be resolved accurately if the measurement resolution is some order-one constant multiplied by η. Knowing whether this constant is 1 or 9 is critical to designing experiments to accurately measure velocity gradients in turbulent flow at a scale relevant to microscopic organisms.

Several studies of the effect of resolution on the accuracy of PIV measurements of Eulerian fluid parameters in idealized turbulence showed that coarser spatial resolution reduces the magnitude of velocity gradients and the frequency of measured high-magnitude velocity gradient, vorticity, and dissipation events (Worth et al. 2010; Buxton

et al. 2011). Studies suggest that an inter-vector spacing of $\Delta x = 3\eta$ is necessary to accurately measure time-averaged variance of velocity gradients (Antonia et al. 1993, 1994), $\Delta x = \eta$ could be necessary to measure the temporal variance of velocity gradients (Buxton et al. 2011), and $\Delta x = ½\ \eta$ is needed to accurately measure the probability density function (PDF) of the velocity gradients (Donzis et al. 2008). In turbulent flow, the PDF of the velocity has wide tails, which means that very high-magnitude events occur more frequently than they would for a variable with a Gaussian distribution (Jimenez 1997). Accurately capturing these high-magnitude events, which are likely to affect plankton and their behavioral responses, should be an important part of Lagrangian analyses to quantify the temporal pattern of velocity gradients that plankton experience when carried in turbulent flow. As far as we are aware, the effects of PIV resolution in realistic flows, such as the benthic boundary layer flows we consider, have not been studied, nor has the effect of PIV resolution been measured along Lagrangian trajectories.

Research system

We used larvae of benthic marine invertebrates (size range ~0.1–1 mm) as model organisms to explore the interaction of microscopic organisms with the fine-scale aspects of ocean flows that they encounter because larval interaction with the fluid flows around them is critical for determining where they settle (reviewed by Abelson and Denny 1997; Koehl 2007) and because the larvae of some species have been shown to react to the fluid flow around them (Fuchs et al. 2004, 2013, 2015; Wheeler et al. 2013, 2015). The process of larval settlement is an important factor affecting the meta-population dynamics of many types of marine animals as well as the structure of benthic marine communities (reviewed in McEdward 1995).

Our study focused on larval settlement into 'fouling communities,' the assemblages of organisms living on surfaces (including docks and ships) in harbors, bays, and estuaries. Fouling communities have been used as systems for studying ecological succession, the process by which communities are established and develop over time (e.g., Sutherland and Karlson 1977; Bram et al. 2005; Greene and Grizzle 2007), and for investigating the process of larval settlement (reviewed by Koehl 2007). Boat and ship wakes are common occurrences in such locations and are good examples of the fluid flows larvae may experience there while settling. We therefore focus on these types of flow.

Objectives of this study

The goal of the research reported here was to determine the variations in water motion encountered by individual zooplankters along their trajectories in realistic ambient flow conditions. To do this, we quantified the temporal patterns of velocity gradients and accelerations encountered by simulated microscopic larvae carried in turbulent boundary layer flow across the complex topography of a fouling community exposed to waves. The specific objectives of our study were:

1. To determine the effects of some examples of different ambient water flow conditions typical of harbors on the temporal patterns of flow encountered by a larva near a fouling community.
2. To quantify the consequences of various characteristics of larvae (buoyancy, sensitivity to flow signals, time required to react to flow signals) on how larvae are affected by the temporal patterns of flow signals experienced.
3. Because we used PIV to quantify the complex changing flow fields in which the larvae were moving, a third objective of our study was to determine how the spatial resolution of the PIV affected the measured Eulerian flow fields, the calculated larval trajectories through those flow fields, and the Lagrangian patterns of accelerations and velocity gradients encountered along these trajectories.

Methods

Field measurements of water flow

To determine a realistic range of flow conditions near fouling communities, we measured water velocity profiles near fouling communities on docks at several sites in Pearl Harbor (Oahu, HI). Fouling communities in Pearl Harbor are subjected to slow water currents and waves due to wind chop and the wakes of boats and ships, which is typical of flow measured near fouling communities in other harbor locations (Okamura 1984; Hunter 1988; Schabes 1992; Koehl 2007). We used an acoustic Doppler velocimeter (Sontek 16 MHz MicroADV; sampling volume = 0.25 cm^3; sampling rate = 25 Hz) to measure the water velocity profiles near fouled panels (25.4 cm × 30.5 cm) on a dock in Pearl Harbor, HI (details given in Holm et al. 2000). We also measured similar water velocity profiles near fouled panels at a different site in Pearl Harbor using an electromagnetic flowmeter (Marsh-McBirney Model #523), as described by Koehl (2007) and Koehl et al. (2013).

So that we could mimic in our laboratory flow tank the waves and small-scale stochastic fluctuations in water velocities to which fouling communities were exposed in the field, we calculated the power spectral density of each field velocity record by Welch's method (examples in

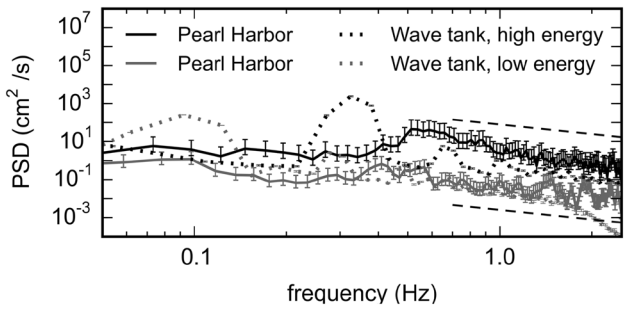

Fig. 1 Power spectral density (PSD) for examples of water flow measured across fouling communities on docks at different sites in Pearl Harbor, HI, and for the flume flow conditions we used. *Dashed straight lines* above and below the high-frequency data indicate a −5/3 slope, which is characteristic of the inertial subrange of turbulent flow (Davidson 2004; Thorpe 2007). *Error bars* indicate 95 % confidence intervals (CIs) and are approximately the size of the thickness of the *dashed line* for wave tank data. Both PSDs and CIs were computed using Welch's method in MATLAB using half overlapped windows of sizes 32 s for lower energy waves in the flume, 18 s for higher energy waves in the flume, 41 s for the field data represented with the *solid black line*, and 51 s for field data represented by the *solid gray line*. PSD and CIs for the flume data were calculated from several runs concatenated in phase: three runs of 32 s for the lower energy wave flow, and five runs of 18 s for the higher energy waves flow. The peak water speeds of the waves in the field due to ship wakes could be as high as 10–20 cm s^{-1} (Koehl et al. 2013), but the examples for the spectra shown here had mean peak velocities of 7.5 cm s^{-1} (SD = 2.5, n = 63 waves; *black line*) and 2.1 cm s^{-1} (SD = 0.4, n = 106 waves; *gray line*). The flume higher energy waves (*black dotted line*) had a mean peak velocity of 22 cm s^{-1} (SD = 0.7, n = 29 waves), and the flume lower energy waves (*gray dotted line*) had a mean peak velocity of 5.5 cm s^{-1} (SD = 0.15, n = 8 waves)

Fig. 1; wave frequencies ~0.1–0.6 Hz for these examples) (Welch 1967; Rabiner and Gold 1975). Such spectra indicate how much of the variation in velocity is due to fluctuations at different frequencies.

Wave tank experiments

We used an oscillating-flow flume to produce two flow regimes that fell within the range of waves we recorded in Pearl Harbor (0.1–1.2 Hz, 2–20 cm s^{-1} peak velocity) and that mimicked the fine-scale stochastic velocity fluctuations we measured in the field: 'lower energy waves' had a lower frequency (~0.1 Hz), slower peak velocities (~5 cm s^{-1}), and less energetic stochastic fluctuations than did 'higher energy waves' (~0.3 Hz, ~20 cm s^{-1}). Examples of spectra for field and laboratory flow are shown in Fig. 1. The stochastic velocity fluctuations in the field and flume were a combination of turbulence and interacting eddies shed from the complex bottom topography of the fouling community. Our flume design (Fig. 2) is like that described by Robinson et al. (2007). Panels on which

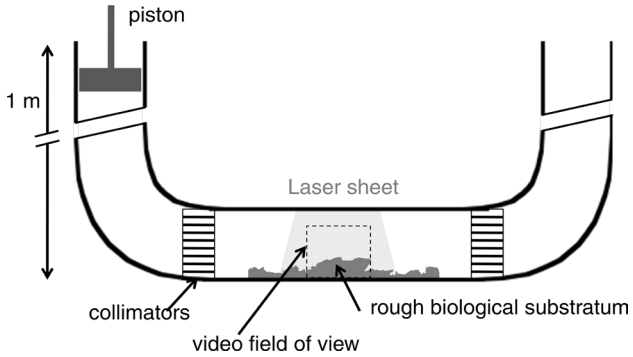

Fig. 2 A diagram showing the experimental setup of the oscillating-flow flume (not to scale)

fouling communities had developed in Pearl Harbor were attached to the floor of the working section. We used freeze-dried (in a Vertis Freezemobile 12ES Lyophilizer) fouling communities painted black in order to retain accurate fine-scale topography while avoiding reflections of the light from the laser.

In order to measure the flume flow fields for use in our simulations, we used PIV to map instantaneous water velocity fields. In order to minimize motion blur of the marker particles, videos of the lower energy wave flow were made at 63 frames per second (980 × 850 pixels resolution), and of the faster higher energy wave flow at 111 frames per second (1100 × 900 pixels resolution). We used PIV software (MatPIV 1.6.1) to calculate water velocities for each pair of frames. In order to remove spurious vectors, vectors that differed by more than 1.5 standard deviations from their immediate neighbors were removed in the higher energy wave flow, and those that differed from their neighbors by more than 2.0 standard deviations were removed in the lower energy wave flow. No spatial filtering was done, in order to preserve the highest velocity gradients present in the flow field, though a temporal Butterworth filter with cutoff frequencies of 2 Hz for the lower energy wave and 11.1 Hz for the higher energy wave flow conditions was applied at each PIV grid position through time to remove noise in the temporal domain (rational explained in Biewener and Full 1992). Our PIV experimental conditions are within the range recommended for accurate PIV: The average particle size was 3–7 pixels, somewhat larger than the ideal of 2 pixels; our dynamic range was 6–8 bits/pixel, well above the 4 that is needed (See Raffel et al. 1998 Ch. 5 for more details of recommended parameter ranges) (see Online Resource 1 for an example experimental video with PIV vectors).

To test the effects of PIV resolution, flow fields of three different resolutions were created from the same initial video by using PIV sampling windows of 32 × 32 pixels, 64 × 64 pixels, and 128 × 128 pixels with windows 50 %

overlapped. At all resolutions a multi-pass PIV algorithm with three passes was used in order to detect large displacements in fast flow (initial window size of 64 × 64 pixels used for the 32 × 32 pixel resolution, and initial window size of 128 × 128 pixels used for the other two resolutions). The distance between adjacent velocity vectors was 2.01, 4.02, and 8.03 mm for the three resolutions in the lower energy wave flow, and 1.76, 3.52, and 7.03 mm in the higher energy wave flow. In the rest of the paper, we will refer to these three resolutions as fine, medium, and coarse resolution, respectively. If measurements matched between the fine and medium resolution, we concluded that both resolutions were sufficient to accurately make that measurement. If measurements did not match, we concluded that the medium resolution was insufficient, but cannot make a determination about the fine resolution. Our lowest resolution of 32 × 32 pixels was chosen such that it would still achieve the necessary particle seeding density of 5–10 particles per integration window for accurate PIV (Raffel et al. 1998). Our fine resolution had on average 11–12 particles per window with a lower bound of around 8.

An example of an instantaneous PIV flow field from each resolution are shown in Fig. 3. The four spatial gradients that can be determined in two dimensions ($\partial u/\partial x$, $\partial w/\partial z$, $\partial u/\partial z$, and $\partial w/\partial x$, where u is the velocity in the x direction, and w is the velocity in the z direction) were calculated from the measured flow field using central differences. In the flume, the x direction was the direction in which waves propagate and the z direction was vertical.

General characteristics of the flow for each flow type and at each resolution are listed in Table 1 along with a comparison to idealized flows. We calculated the dissipation rate, ε, for each PIV grid location at each time according to $\varepsilon = 0.5\ (u')^3/L$ where 0.5 is an empirical constant, u' is the fluctuating velocity, and L is a size scale corresponding to the most energetic motions in the flow; we use $L = 5.5$ cm, half of the flume's smallest dimensions (de Jong et al. 2008). We then calculated the Kolmogorov length, η, at each PIV grid location at each time point according to $\eta = (\nu^3/\varepsilon)^{1/4}$ (Pope 2000). For the sake of calculating ε and η, we found u' by removing the wave velocity from our PIV flow fields using a notch filter from 0.1 to 0.7 Hz in higher energy waves and 0.04–0.3 Hz in lower energy waves flow. The scaling argument for ε above has been shown to be accurate to within a factor of two in isotropic homogeneous turbulence, which means calculations of η should be accurate to within 20 % (Variano and Cowen 2008; de Jong et al. 2008). Errors in our realistic wavy flows might be somewhat different, though we are aware of no other established techniques for calculating ε and η in turbulent, wavy flow. We chose to use the scaling argument above rather than direct calculation of ε from measured velocity gradients since under-resolved PIV results in low estimates for ε, with errors that would likely depend on spatial location relative to the substratum for our realistic flows (Tanaka and Eaton 2007; de Jong et al. 2008). To compare our real flows to idealized isotropic homogeneous turbulent flows, we also calculated the approximate variance of transverse velocity gradients as $\varepsilon/(7.5\nu)$ and longitudinal velocity gradients as $\varepsilon/(15\nu)$ in isotropic homogeneous turbulence, where ν is the kinematic viscosity of water (Pope 2000).

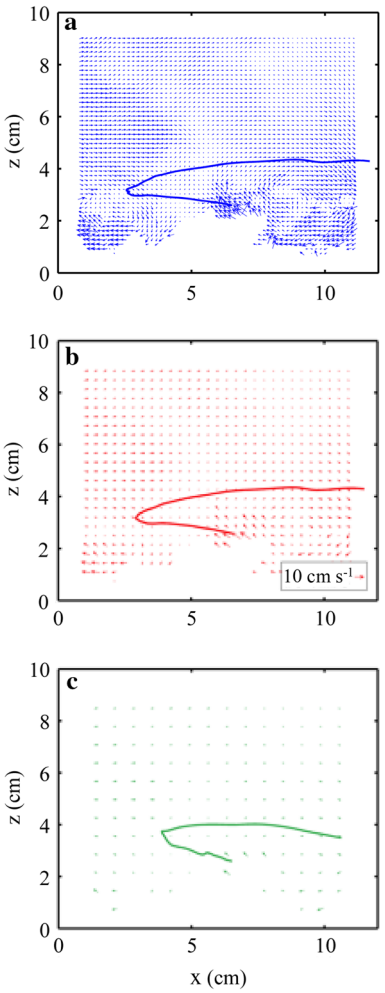

Fig. 3 Example frame from PIV at each of the three resolutions, including one example larva trajectory that was started at the same location and time in each of the three flow fields. While the PIV vectors are an example from a single time point, the overlaid trajectories result from simulating the motion of a passive tracer in the measured PIV flow field that changes in time as described in Eq. 1. The duration of this trajectory is 1.3 s. Missing vectors at the *bottom* are due to the presence of the rough biological substratum. This example is from the higher energy wave flow condition. **a** PIV with fine resolution. **b** PIV with medium resolution. **c** PIV with coarse resolution. *Colors* for each resolution match those in Figs. 5, 6, and 7. All PIV vectors have the same scale as shown in **b**

Table 1 General characteristics of flow measured in the wave tank using PIV

	Δx (cm)	$<\|u\|>$ cm s^{-1} (95 % CI)	$<\|w\|>$ cm s^{-1} (95 % CI)	$<\|\partial u/\partial x\|>$ (s^{-1}) (95 % CI)	$<\|\partial u/\partial z\|>$ (s^{-1}) (95 % CI)	$<\|\partial w/\partial x\|>$ (s^{-1}) (95 % CI)	$<\|\partial w/\partial z\|>$ s^{-1} (95 % CI)	$<\varepsilon>$ (cm^2 s^{-3}) (min–max)	$<\eta>$ (cm) (min–max)
Lower energy wave fine	0.201	2.982 (2.981–2.983)	0.3213 (0.3208–0.3217)	0.3937 (0.2932–0.3943)	0.614 (0.613–0.615)	0.2955 (0.2951–0.2959)	0.2902 (0.2898–0.2906)	0.01 (0.001–0.1)	0.2 (0.1–0.3)
Lower energy wave medium	0.402	2.924 (2.921–2.926)	0.2891 (0.2883–0.2897)	0.2674 (0.2668–0.2681)	0.426 (0.425–0.428)	0.2122 (0.2116–0.2129)	0.2011 (0.2006–0.2017)	0.01 (0.001–0.1)	0.2 (0.1–0.3)
Lower energy wave coarse	0.803	2.902 (2.896–2.908)	0.263 (0.262–0.264)	0.1597 (0.1588–0.1604)	0.269 (0.267–0.270)	0.1404 (0.1396–0.1411)	0.1249 (0.1245–0.1255)	0.01 (0.001–0.09)	0.2 (0.1–0.3)
Higher energy wave fine	0.176	11.705 (11.700–11.712)	1.158 (1.157–1.159)	2.169 (2.167–2.172)	3.318 (3.314–3.324)	1.692 (1.690–1.694)	1.638 (1.635–1.639)	1 (0.2–10)	0.06 (0.03–0.09)
Higher energy wave medium	0.352	11.587 (11.578–11.600)	1.115 (1.113–1.117)	1.538 (1.533–1.541)	2.59 (2.58–2.60)	1.160 (1.157–1.162)	1.075 (1.073–1.077)	1 (0.2–20)	0.07 (0.03–0.09)
Higher energy wave coarse	0.703	11.32 (11.29–11.34)	0.993 (0.990–0.996)	1.042 (1.037–1.048)	1.926 (1.916–1.935)	0.656 (0.654–0.659)	0.590 (0.587–0.592)	2 (0.1–20)	0.07 (0.03–0.1)

Symbols surrounded by < > indicate averages over both space and time. 95 % confidence intervals (CI) are calculated using bootstrapping with replacement to generate 100 bootstrap samples of the same size as the original. The minima and maxima listed with ε and η are the maxima (max) and minima (min) comparing different spatial locations after time-averaging each spatial location. For comparison, in isotropic homogeneous turbulence with the ε values for fine-resolution flow given below, we expect root-mean-square longitudinal velocity gradients of approximately 0.3 s^{-1} in the lower energy and 3 s^{-1} in the higher energy flow and transverse velocity gradients of 0.4 and 4 s^{-1} in the lower and higher energy flows, respectively

Calculation of larval trajectories in measured water flow

To determine the temporal patterns of velocity gradients and accelerations the larvae encountered, larvae were modeled as passive tracers in the time-varying flow fields measured in the wave tank with PIV. In order to determine whether the spatial resolution of the PIV measurements changed larval trajectories or the temporal pattern of velocity gradients and accelerations they experienced along those trajectories, we ran the model using the PIV measurements taken at different resolutions (fine, medium, and coarse). For all flow conditions and PIV resolutions, we seeded the flow field with 2000 larvae at random locations at a steady rate in time (6 larvae/frame for the first 350 frames in higher energy wave flow and 3 larvae/frame for the first 650 frames at the lower energy wave flow). Larvae were seeded over time as well as space because they can be swept out of the field of view and we wanted to sample all phases of the wavy flow. The same initial start locations and times were used at all three PIV resolutions for each flow condition. The position of the larvae in frame n was determined as:

$$\mathbf{x}_n = \mathbf{x}_{n-1} + \mathbf{u}_{n-1}(\mathbf{x}_{n-1})\Delta t + \mathbf{v}_g \Delta t \quad (1)$$

where $\mathbf{x}$ is the 2D vector location of the larva, $\mathbf{u}_n$ is the 2D fluid velocity in frame n as measured using PIV, n and $n-1$ refer to the frame number, Δt is the time between adjacent frames in the video (16 ms for lower energy wave and 9 ms for higher energy wave videos), and $\mathbf{v}_g$ is a sinking or rising velocity for nonneutrally buoyant larvae or eggs. The expression $\mathbf{u}_{n-1}(\mathbf{x}_{n-1})$ indicates that the velocity field in frame n−1 was evaluated at position $\mathbf{x}_{n-1}$, the position of the larvae in frame n−1, not that the two values were multiplied. The velocity, $\mathbf{u}_n$, was interpolated from the PIV grid to the location of the larva using one-dimensional cubic spline interpolation in each dimension (Mathews and Fink 1999).

We chose completely passive neutrally buoyant larvae as the most simple model for a first analysis of resolution effects by setting $\mathbf{v}_g = 0$. We also ran the model for particles with a sinking velocity of 1.5 mm s^{-1}, which is similar to reported sinking velocities for larvae of molluscan veligers (Chia et al. 1984; Hadfield and Koehl 2004; Chan 2012), polychaetes (Butman et al. 1988), and various crustaceans (Chia et al. 1984). Calculations were also performed for particles with a rising velocity of 1.5 mm s^{-1}, which is in the range of rising speeds for eggs of some sea urchins (Thomas 1994) and corals (Szmant and Meadows 2006). Simulated trajectories were ended when the larvae or eggs exited the field of view or touched down on the substratum at the bottom. We removed any trajectories with durations shorter than 0.08 s. This gave $n = 1931$ larval trajectories

for the lower energy wave flow and $n = 1802$ trajectories for the higher energy wave flow at all three PIV resolutions.

The linear combination of pathline-following with sinking or rising that we used in Eq. 1 is a reasonable first approximation and a practical place to start investigating the effects of density. While this is accurate for small, neutrally buoyant larvae that do not move relative to the fluid, nonneutrally buoyant larvae may also be moved preferentially into or out of eddies due to fluid acceleration (Maxey and Riley 1983; Toschi and Bodenschatz 2009). For tractability of calculation, we also neglect other fluid forces on the larvae that are negligible for bodies that move relative to the fluid at low Reynolds number (Maxey and Riley 1983).

To quantify the effect of resolution on trajectories, we use the trajectories of larvae calculated starting from the same points in the water column but using velocities that were measured using the fine, medium, or coarse PIV resolutions. We then calculated the difference in the endpoint of the trajectories calculated in fine versus medium and fine versus coarse flow as a function of time along the trajectory. We then normalized these differences by the length of the fine trajectory as a function of time along the trajectory to get deviation as a percent of the total distance traveled. This percent deviation was then averaged for all the larvae to create an average percent deviation as a function of time along the trajectory. This average was only computed if at least 10 trajectories were available, which limited the time along trajectories to less than 1.3 s in higher energy wave flow and less than 4.9 s in lower energy wave flow. A similar calculation of average percent deviation along trajectories was performed to determine the effect of larval buoyancy on larval trajectories by performing the same analysis, but comparing larvae with a sinking or rising velocity with neutrally buoyant larvae, all started in the same location in the same flow field.

One limitation of our method is that the flow fields we measured and the larval trajectories we simulated were both two dimensional. However, we expect this to reflect accurately the largest spatial gradients in the flow field because we captured flow in the direction of wave propagation (x) which has the largest mean flow velocity, and in the direction that cuts across the benthic boundary layer normal to the surface of the fouling community (z), which has the largest mean velocity gradient. Because of this, and since magnitudes of the three components of velocity fluctuation in shear layers are typically roughly the same (Townsend 1980; Raupach et al. 1991), we expect the flow velocities, velocity gradients, and accelerations in the direction (y) not captured in our videos should be comparable to or smaller than in the two directions we measured. The accelerations we measure, however, are a lower bound, as they do not include any temporal changes in velocity in the y-direction.

Calculation of temporal patterns of mechanical signals along larval trajectories and effect on larvae

Once we used the above procedure to determine the trajectories larvae follow in the flow, we then determined the temporal pattern of body accelerations and spatial gradients in the flow field that they experienced along these trajectories. Accelerations of larvae were determined from fluid velocities interpolated to the larva's position and with central differences in times (Mathews and Fink 1999). Spatial gradients along larval trajectories were interpolated to the larva's position using one-dimensional cubic spline interpolation in each dimension.

We explored how larvae or eggs might be affected by instantaneous flow conditions that they encountered along their trajectories by assuming that they are affected by gradients or accelerations above threshold values. Effects could include a cessation or change in swimming or feeding behavior (Finelli and Wethey 2003; Fuchs et al. 2004, 2013), though none was included in this model, a physiological change, such as an increase in larval development rate (Gaylord et al. 2013), or damage (Thomas and Gibson 1990). We calculated the fraction of time that larvae were affected by the flows measured at the three different resolutions. The simulated larvae were assigned a threshold for one fluid flow parameter (e.g., $\partial u/\partial z$ or a) and were considered to be affected when the value of that parameter along their trajectory was above the threshold value. In our simulation, no change in larvae behavior was induced by the flow that would alter the larval trajectory, although this type of coupling would be an interesting avenue for further study.

To have our simulated larvae affected by the flow in the way similar to real marine larvae, the flow parameter ($\partial u/\partial z$ or a) had to remain above the threshold for a time period long enough for a larva to detect and react to the signal (t_{react}) for the larva to be affected by the flow. We also incorporated a lag time (t_{resume}) for a larva to resume its nonreacting behavior and stop being affected by the flow after the flow signal fell below threshold. An example of the time that a single larva spends affected by the flow along its trajectory is shown in Fig. 4. Because veliger larvae retract their velar lobes when disturbed, they provide a system in which we could measure t_{react} and t_{resume} (Table 2). We report here our results from simulations using typical times for veliger reactions to mechanical stimuli: $t_{\text{react}} = 0.08$ s and $t_{\text{resume}} = 1.2$ s. We ran simulations using other lag times and found that our qualitative results on the sensitivity of larval experience to the resolution of the flow field were not affected by changes in these times in the range $0.06 \text{ s} < t_{\text{react}} < 0.08$ s and $0.03 \text{ s} < t_{\text{resume}} < 3.6$ s (see Table 2 for examples of measured t_{react} and t_{resume}).

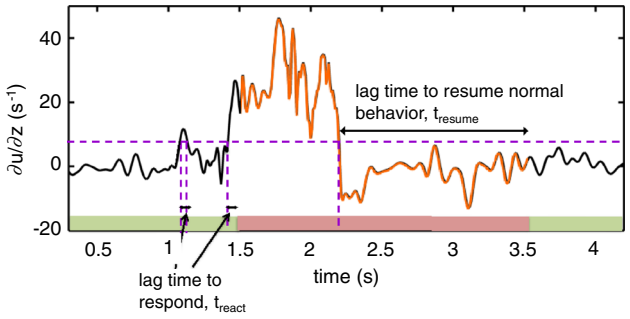

Fig. 4 Value of $\partial u/\partial z$ as measured along a larval trajectory in the fine-resolution PIV flow field for the higher energy wave flow condition. The *dashed purple horizontal line* is an example of a threshold value above which this larva would be affected by the hydrodynamic signal. The *dashed purple vertical lines* indicate when the signal is at the threshold. The *orange portion* of the $\partial u/\partial z$ line indicates when this simulated larva would be affected by the $\partial u/\partial z$ signal according to our model ($t_{react} = 0.08$ s and $t_{resume} = 1.2$ s). The *colored bars* at the *bottom* of the graph indicate the time that this larva spends affected (*red*) and not affected (*green*)

Results

Effects of spatial resolution of PIV measurements

Table 1 lists some of the general characteristics of the two flow regimes (lower energy wave and higher energy wave) used in this study; these statistics were calculated using PIV data taken at fine, medium, and coarse spatial resolutions. The mean absolute values for the horizontal and vertical flow velocities averaged over space (all spatial points in an instantaneous flow field) and time (all instants in a video) were significantly different (95 % confidence intervals did not overlap) between the different PIV resolutions, with higher values at finer resolutions. Similarly, the magnitudes of the velocity gradients averaged over both space and time were significantly greater for finer PIV resolutions. In contrast, PIV resolution did not change the Kolmogorov scale (η) or rate of dissipation of turbulent kinetic energy (ε) averaged over space and time. Velocity gradient estimates for isotropic homogenous turbulence with the same ε as our flow match our measured velocity gradients within a factor of two, which is approximately the accuracy of our ε values, except for the case of $\partial w/\partial x$. This longitudinal velocity gradient for w, the flow velocity perpendicular to the substratum, is lower than the estimate by more than a factor of two, which may be explained by the fact that perpendicular flows are suppressed by the presence of the substratum, so w and its gradients should be smaller than in unbounded isotropic homogenous flow.

The variability of various aspects of the water flow is better shown by the probability density functions (PDFs) for these parameters. Examples of the PDFs for vertical water velocities (w) and for the vertical spatial gradients in horizontal flow velocity ($\partial u/\partial z$) are shown in Fig. 5, calculated using PIV data with different spatial resolutions. When the PDFs of fine and medium resolution overlap, this indicates that our fine and medium PIV data both have sufficient resolution to accurately measure the vertical velocity. There is a near overlap of the PDFs of vertical velocities measured at the medium and fine PIV resolutions in both flow conditions (Fig. 5a,c). That the PDF for the coarse-resolution PIV is different in this example indicates that the coarse resolution is not well enough resolved to accurately measure vertical velocity. We saw similar results for the PDFs of horizontal velocity, u, and conclude that the fine and medium PIV resolutions were adequate to measure velocity flow conditions and that errors are likely to be small.

Although the PDFs of velocities nearly overlap for the three resolutions, the PDFs of the spatial gradients in velocity do not. The lack of overlap for any of the lines in Fig. 5b,d indicates that neither the medium nor coarse PIV resolutions were sufficient to measure Eulerian spatial gradients in velocity such as $\partial u/\partial z$. We saw a similar lack of overlap for the other spatial gradients, $\partial u/\partial x$, $\partial w/\partial z$, and $\partial w/\partial x$ and conclude that the medium and coarse PIV resolutions are insufficient to accurately measure spatial gradients in both lower energy wave and higher energy wave flow fields. Without even higher resolution PIV, we cannot say whether the fine resolution we tested is sufficient. The parts of the PDFs that are most different between

Table 2 Examples of reaction times (t_{react}) and resumption times (t_{resume}) for various marine molluscan veliger larvae

Species	Stimulus	t_{react} (SD, n)	t_{resume} (SD, n)	Source
Phestilla sibogae (sea slug)	Water acceleration ($d\mathbf{u}/dt = 6$–25 cm s^{-2})	0.1 s (0.1, 4)	0.8 s after water motion stopped (0.6, 11)	Videos of larvae in microfluidic device (R.E.P. and M.A.R.K., unpubl. data)
Phestilla sibogae	Bump into obstacle	0.08 s	1.2 s	Online Resource 2 (R.E.P., unpubl. data)
Phestilla sibogae	Dissolved settlement cue	1.1 s (0.7, 8)	0.8 s (2.9, 7)	Hadfield and Koehl (2004)
Ostrea sandvicensis (oyster)	Spontaneous retraction	na	1.3 s (0.3, 3)	Videos of larvae in still water (R.E.P., unpubl. data)

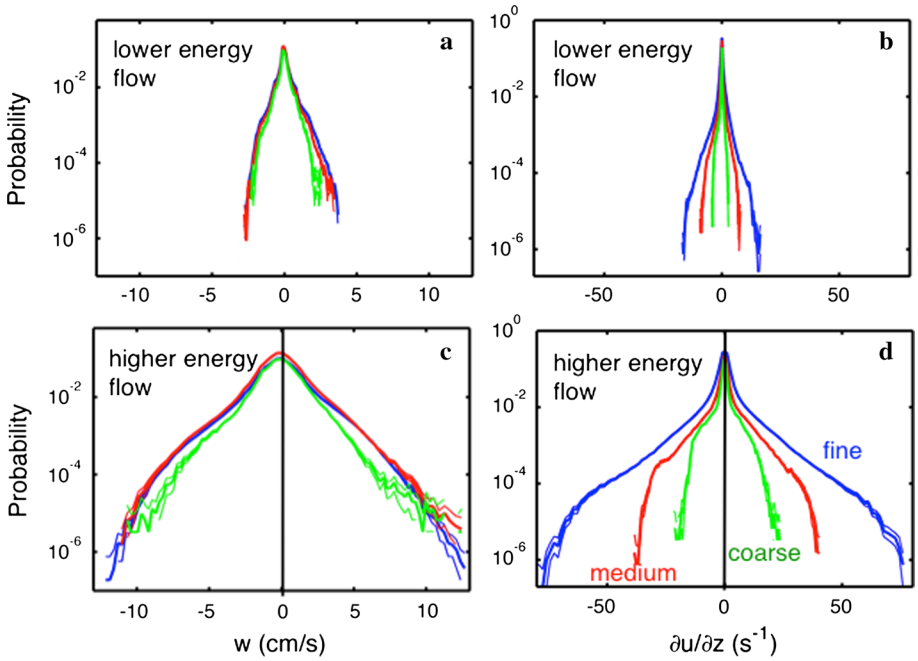

Fig. 5 Probability density functions (PDFs) for the flow field measured with PIV. The *three lines* are PDFs from the three different resolutions of PIV. *Blue* fine PIV. *Red* medium PIV. *Green* coarse PIV. *Thinner lines* represent 95 % confidence intervals determined using bootstrapping. Probabilities of measuring values of **a** vertical velocity, w, in the lower energy wave flow field, **b** one spatial gradient, $\partial u/\partial z$, in the lower energy wave flow field. **c** Vertical velocity, w, in the higher energy wave flow field. **d** One spatial gradient, $\partial u/\partial z$, in the higher energy wave flow field. PDFs were made by first creating a histogram of the measured value of the velocity or spatial gradient at all locations in all frames of the PIV flow field, then dividing by the total number of values. Each histogram has 100 bins. Confidence intervals were determined using bootstrapping with replacement to generate 1000 replicate data sets

the three PIV resolutions are the tails, indicating that at the coarser resolutions we are missing mainly low-probability, but high-magnitude, events. Do these infrequent but large events significantly change the temporal pattern of mechanical signals to larvae traveling in these flow fields? To answer this question we switch to a Lagrangian framework to examine measurements taken along larval trajectories.

Since the PDFs reveal that our PIV resolutions are sufficient or nearly sufficient to measure velocity, we expect that larval trajectories should be accurate at all 3 resolutions. Indeed, as illustrated by the example shown in Fig. 3, PIV resolution had little effect on larval trajectories. We found that simulated larval trajectories measured at coarse resolution separated from those measured at fine resolution on average less than 9 % of the distance along the trajectory, and those measured at medium resolution separated on average less than 5 % of the distance along the trajectory for trajectories in both lower and higher energy wave flows.

We also explored the effect of the spatial resolution of PIV on the temporal patterns of velocity gradients and accelerations along simulated larval trajectories. An initial qualitative sense for whether the resolution of the flow field changes our predictions of larval experience can be seen in Fig. 6, which shows the temporal pattern of accelerations and velocity gradients experienced along example larval trajectories calculated using the three PIV resolutions. At the best resolution (fine), both the velocity gradients (Fig. 6a) and the accelerations (Fig. 6b) reached higher magnitudes and fluctuated more rapidly in time than at lower resolutions. As the resolution was decreased, the trace became smoother, reaching lower peak magnitudes and varying more slowly. By looking at the example of a threshold above which larvae would be affected by the flow (shown as a dashed line in Fig. 6a), it is clear that analysis using fine-resolution PIV data predicted more time affected than did analysis using medium resolution. The effect is so strong that coarse resolution in this example produced no time affected.

In order to make this analysis more quantitative, we computed the fraction of time each larva spent affected by velocity gradients or accelerations as it traveled along its trajectory through each flow field at the three PIV resolutions. We then calculated the mean of this fraction of time for all larvae and a range of thresholds. We found that, except at very low thresholds, there was a significant difference (i.e., 95 % confidence intervals did not overlap) between the three PIV resolutions in the fraction of time that larvae spent affected by velocity gradients (Fig. 7). This difference was most pronounced for those simulated

larvae with higher thresholds. For instance, at a threshold of ~22 s^{-1} (straight purple line in Fig. 7c), larvae simulated in the higher energy wave flow measured with fine resolution spent around 2 % of their time affected by the flow, while larvae simulated in the medium-resolved flow spent around 0.4 % of their time affected, and larvae simulated in the coarsest resolved flow spent no time affected by the flow because they never experienced gradients above the threshold for a long enough time to be affected. Since the 95 % confidence intervals do not overlap for the three flow-field resolutions in either higher energy wave or lower energy wave flow, we can conclude that our coarse and medium PIV resolutions were not sufficient to accurately measure larval experience of spatial gradients in these flow conditions.

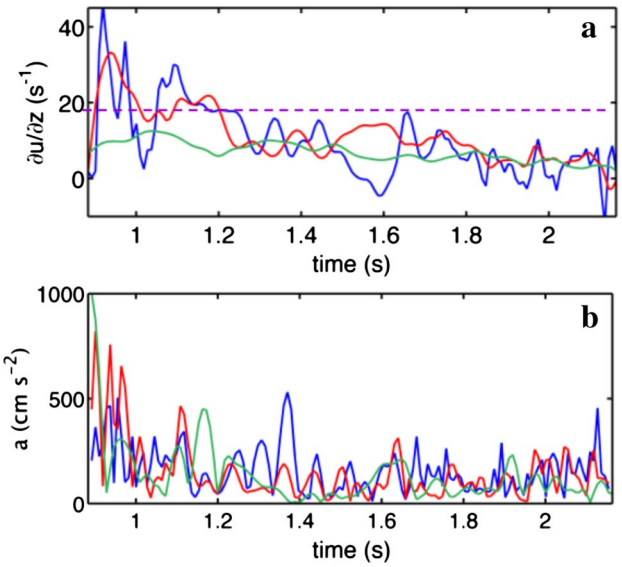

Fig. 6 Value of $\partial u/\partial z$ (**a**) and magnitude of acceleration (**b**) as measured along a larval trajectory in the higher energy wave flow field at three resolutions. The larval trajectory can be seen in Fig. 3. The *three lines* are from larval trajectories in the three different resolutions. *Blue* fine PIV. *Red* medium PIV. *Green* coarse PIV. The *dashed purple line* is an example of a threshold value above which this larva would be affected by the hydrodynamic signal

Unlike the velocity gradient, the fraction of time larvae spend affected by accelerations at the three different PIV resolutions is similar. The 95 % confidence intervals overlap between fine and medium resolutions at all thresholds for both flow conditions, and the 95 % confidence intervals for fine and coarse resolutions overlap for all thresholds in the higher energy waves and nearly all thresholds for lower energy waves (Fig. 7b,d). These results indicate that the fine and medium PIV resolutions were sufficient for measuring larval experiences of acceleration in both of these flow fields.

The time that larvae take to react to mechanical signals, and the time to resume normal behavior after the signal ends also determine the time they are affected by flow. We found that changes in reaction and resumption times in the range 0.06 s $< t_{react} <$ 0.08 s and 0.03 s $< t_{resume} <$ 3.6 s did not alter the effects of PIV resolution on the mean fraction of time that larvae spend affected by flow. However, if t_{react} falls outside this range, the fraction of time affected by acceleration does differ between the three PIV resolutions (95 % CI's overlap

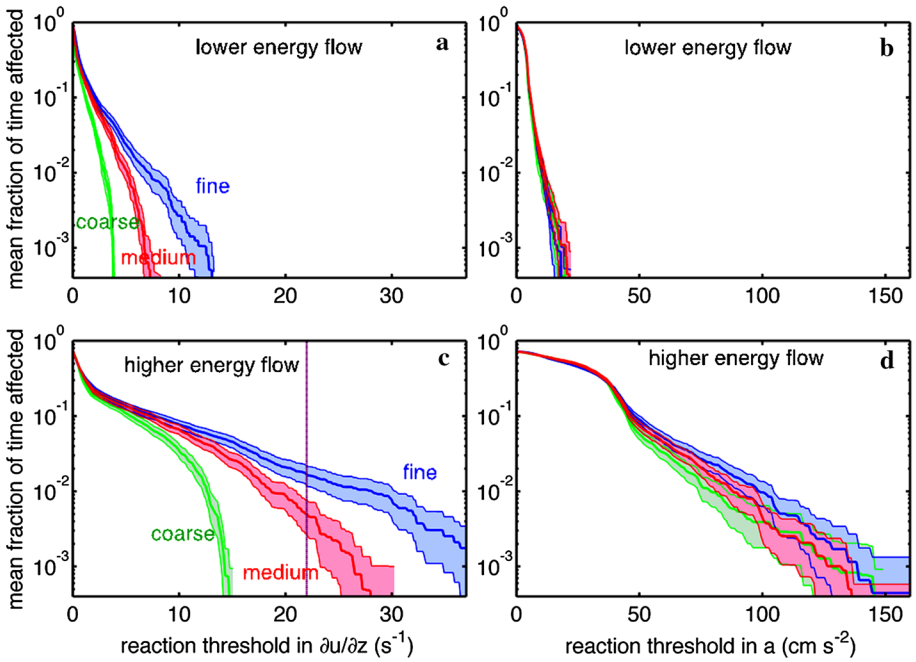

Fig. 7 Mean fraction of time larvae spend affected by velocity gradients and accelerations in flow. Varying thresholds above which larvae would be affected are shown on the *x*-axis. The *three lines* represent the three different resolutions as labeled; the *shaded areas* and *lighter lines* are 95 % confidence intervals. *Blue* fine PIV. *Red* medium PIV. *Green* coarse PIV. The *purple line* is an example of a threshold value above which this larva would be affected by the hydrodynamic signal

for all three resolutions or none in the lower energy flow, rather than only medium and fine overlapping).

Temporal patterns of acceleration and spatial gradients in velocity encountered by larvae with different sensitivities

We use the finest resolution PIV data (blue lines in Figs. 3 and 5, 6, 7) to investigate the temporal patterns in the accelerations and spatial gradients in velocity along the trajectories of our simulated larvae. Examples of the $\partial u/\partial z$ and the accelerations encountered by a larva in the higher energy wave flow regime are plotted as a function of time in Fig. 6. It is obvious that the magnitude of velocity gradients and accelerations encountered by a larva fluctuate rapidly, with peaks lasting just fractions of a second. Our Lagrangian analysis of simulated larvae showed that larvae are not subjected to steady velocities or velocity gradients when traveling in realistic wavy, turbulent flow.

We computed the fraction of time each larva spent affected by velocity gradients or accelerations, as it traveled along its trajectory through the lower energy wave or the higher energy wave flow field, and then averaged for all larvae in each flow condition. Since the thresholds above which marine larvae of different species react (e.g., by being damaged, by changing behavior) are not yet known, we did our computation for a range of possible thresholds. In Fig. 7, the fraction of time larvae were affected is plotted as a function of the threshold magnitude of a velocity gradient or of acceleration required for larvae to be affected by the flow. The less sensitive a larva was (i.e., the higher the threshold), the smaller the proportion of time it spent affected as it traveled in each of the flow fields we studied. For larvae in higher energy flow that are affected by acceleration, the fraction of time affected decreased little as threshold to be affected was increased for thresholds between 0 and 40 cm s^{-2} but decreased steeply with increases in threshold for higher thresholds; this plateau is not seen for larvae affected by velocity gradients.

We explored the effect of larval reaction time (t_{react}) and resumption time (t_{resume}) on the fraction of time larvae are affected by accelerations or velocity gradients. Increasing t_{react} from 0.04 s to 0.12 s decreases the fraction of time the larvae spend affected for both acceleration and velocity gradient thresholds. This indicates that the temporal pattern of both of these quantities fluctuates substantially on these timescales. Changing t_{resume} has a much weaker effect on the fraction of time larvae spend affected, although increasing this time also increases the fraction of time larvae spend affected by flow.

Effects of larval buoyancy

If a simulated larva sinks or rises (at 1.5 mm s^{-1}), the trajectory it follows through either of the flow fields we studied differs from the trajectory it would have taken if it were neutrally buoyant, as can be seen from some example trajectories plotted in Fig. 8. The relative significance of this difference depends on the flow field. We found that in the lower energy wave flow, sinking larvae separated from rising larvae by distances that were on average 10–20 % of the distance each had travelled along its trajectory. In higher energy wave flow, which carried larvae at higher velocities, the same sinking and rising speeds led sinking larvae to separate from rising larvae on average 2–6 % of the distance along the trajectory. Thus, for the length of time we follow simulated larvae in this study, the trajectories of sinking and rising larvae separate substantially from each other in lower energy wave flow but not in higher energy wave flow. Nonetheless, the mean fraction of time larvae spent affected by spatial gradients in velocity or accelerations was not significantly different between neutrally buoyant, sinking, and rising larvae when measured in either higher or lower energy wave flow measured at any of the three PIV resolutions (the lack of significance determined by overlapping 95 % confidence intervals). Thus, our results above, including those about PIV resolution, are valid for sinking, rising, and neutrally buoyant larvae.

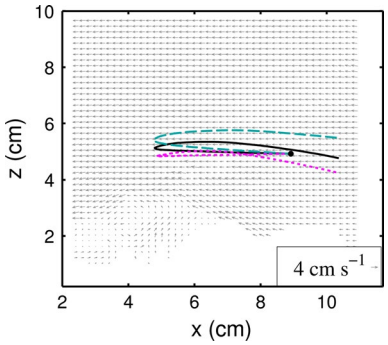

Fig. 8 Example larvae trajectories for the same start location (shown as a *black dot*) for a passive larva (*black solid line*), a larva with 1.5 mm s^{-1} rising velocity (*cyan dashed line*), and a larvae with 1.5 mm s^{-1} sinking velocity (*magenta dotted line*). All larvae are simulated in the lower energy wave flow field at fine resolution according to Eq. 1. One frame of PIV vectors from this flow field is shown in the background for reference

Effects of wave size

The magnitude of the oscillating water velocities in the waves in the higher energy wave flow we tested was greater than in the lower energy wave flow. The mean magnitudes of the horizontal and vertical velocities were roughly 4 times greater in the higher energy wave flow than they were in the lower energy wave flow (Table 1), and the Kolmogorov scale was smaller ($\eta = 0.06$ cm for the higher energy wave, and 0.2 cm for the lower energy wave). Although

mean velocities were only 4 times greater in the higher energy wave flow than in the lower energy wave flow, the fraction of time that larvae spent affected by velocity gradients or accelerations could be as much as an order of magnitude greater in the higher energy wave flow (Fig. 7). In addition, the threshold velocity gradient or acceleration above which larvae were never affected was much higher in the higher energy wave flow than in the lower energy wave flow.

Discussion

Biological implications

Most field and laboratory studies and models of how ocean flows affect planktonic organisms use statistical descriptions of turbulent mixing, currents, or boundary layers to examine physical effects on biological patterns or processes, whereas we studied the fine-scale temporal patterns of variations in water motion encountered by individual zooplankters carried in realistic ambient flow. We quantified the temporal pattern of velocity gradients, and accelerations encountered by individual zooplankters swimming in a turbulent boundary layer across a rough benthic community exposed to different wave conditions. Recent studies both in the field (Sutherland et al. 2011) and in turbulence and wave tanks (Wheeler et al. 2013, 2015; Fuchs et al. 2013) have studied planktonic animals swimming in moving water using video tracking of the animals coupled with simultaneous PIV to determine the motions of the animals *relative to* the water around them. These studies were able to determine how motions of zooplankton were affected both by the movement of the water and by the responses of the animals, but did not magnify the organisms sufficiently to reveal the behavioral mechanisms underlying those responses. In our work, we also use PIV to determine the instantaneous water motions in turbulent flow encountered by individual zooplankters, but rather than tracking actual animals, we use computer simulations of microscopic organisms whose physical characteristics and behavioral responses can be varied. This approach enables us to explore how varying these features of the organisms affects their transport in realistic ocean flow. In addition, quantifying the temporal pattern of flow signals (i.e., accelerations and velocity gradients) encountered by planktonic animals also provides information for the future design of flow devices that expose zooplankters to these realistic flow patterns under a microscope so that details of their behavioral responses (e.g., changes in swimming kinematics, response times) can be measured. For generality, we have quantified for our model larvae the 'time affected' by velocity gradients or accelerations above a threshold value (Fig. 4). In future studies, this abstract term could be replaced with a more concrete description of the actual effect, such as time sinking, time swimming, or time damaged, as appropriate.

By following individual plankters carried in turbulent wavy flow, we found that the accelerations and gradients in velocity that the animals experience fluctuate rapidly (timescale of fractions of a second, much more rapid than the wave period) and often reach values much higher than the mean. Thus, the average velocity gradient values shown in Table 1 (either measured directly or estimated from ε) do not give a full sense of what plankters experience in realistic flow. This matches results from Lagrangian measurements in idealized turbulent flows (Toschi and Bodenschatz 2009) and Lagrangian calculations of instantaneous vorticities in a turbulent boundary layer (Koehl and Cooper 2015). These results caution against the common practice of modeling particle or larval transport using steady time-averaged flow characteristics (e.g., Jeffery 1922; Bretherton 1962; Grunbaum and Strathmann 2003; Gross et al. 1992). For example, calculating larval transport to a coral reef using a time-averaged concentration gradient of a dissolved settlement cue overestimated settlement rates by up to 15 % when compared to calculations using time-varying, fine-scale cue concentrations encountered along larval trajectories (Koehl et al. 2007). Similarly, our results suggest that using steady shear to measure the reactions by, transport of, or damage to plankters (e.g., Mead and Denny 1995; Karp-Boss et al. 2000; Durham et al. 2009; Clay and Grünbaum 2010) may not reveal how these organisms are affected by the short bursts of high velocity gradients they experience in realistic water flow. For example, if swimming larvae are rotated by velocity gradients so that their swimming direction is changed (e.g., Strathmann and Grunbaum 2006; Chan 2012), they experience frequent brief reorientations in random directions in realistic turbulent flow (Koehl and Cooper 2015) that are quite different from the steady reorientation in time that would be predicted by using an average velocity gradient. Our model could be extended to include model plankton that swim through the water that is carrying them and that are rotated by the rapidly varying velocity gradients they encounter.

Laboratory experiments using steady shear cells have shown that planktonic animals can be damaged by velocity gradients above some threshold (Thomas and Gibson 1990; Mead and Denny 1995; Denny et al. 2002). If a brief experience of high acceleration, stretching, or shearing can damage organisms, our demonstration that zooplankters frequently encounter accelerations and velocity gradients much higher than the mean suggests that there may often be conditions that damage organisms even if the mean values of the gradients or accelerations are well below the damage threshold. For example, if we consider larvae in the higher energy wave flow we studied, we find that even

if the threshold for damage in $\partial u/\partial z$ is 10 times above the mean $\partial u/\partial z$ magnitude of 3.3 s^{-1}, larvae still spend around 1 % of their time experiencing velocity gradients above this threshold and thus may be damaged. On the other hand, if the tissues of plankters have the time-dependent mechanical properties typical of many biomaterials (e.g., Vogel 2013), they may be able to resist the brief forces they experience in realistic water flow, but not steady sustained loads of the same magnitude as measured in the laboratory. Thus, our study suggests that intermittent pulses of velocity gradients or accelerations should be used to assess susceptibility to flow-induced damage by various types of zooplankters.

Our study also revealed that a small increase in mean ambient flow velocity (or dissipation rate, ε) can lead to a much larger increase in the fraction of time larvae can be affected by flow. We found that, although mean velocities were only four times greater, and dissipation rates were only five times greater in our higher energy wave flow than in our lower energy wave flow, the fraction of time that larvae spent affected by velocity gradients or accelerations could be as much as several orders of magnitude greater in the higher energy wave flow (Fig. 7). For example, for larvae that are not very sensitive to flow (i.e., affected less than 1 % of the time), the fraction of time spent affected by the flow can be two orders of magnitude greater in the higher energy waves than in the lower energy waves. At some higher thresholds, larvae in the higher energy waves spend up to 2 % of their time affected, while the larvae in the lower energy wave are not affected at all. In addition, we found that the threshold velocity gradient or acceleration above which larvae were never affected was much higher in the higher energy wave flow than in the lower energy wave flow. These results that larvae are affected by flow much more in higher energy wave than lower energy waves are consistent with previous observations of thresholds in the dissipation rate (ε) or fluid acceleration of the water flow above which larval behaviors are observed (Fuchs et al. 2004, 2013, 2015; Wheeler et al. 2015). The differences in flow that we investigated, and which are representative of flow near fouling communities, cover only a small range of the flow variation present between different locations in the ocean. Thus, we expect that the change in the temporal pattern of accelerations and velocity gradients that occur as organisms approach a coastal habitat (Gaylord et al. 2013) could result in a very large change in the fraction of time they are affected by the flow.

Larval characteristics, such as reaction sensitivity, reaction time, and buoyancy, can change their fate in a given water flow field. The lower the sensitivity of larvae to velocity gradients or accelerations (i.e., the higher their threshold values), the smaller the proportion of time they spend affected by flow as they travel in each of the flow fields we studied. We discovered that the relationship between fraction of time affected and sensitivity threshold dropped off more steeply at low thresholds than high thresholds for velocity gradients, but showed the opposite trend for accelerations. This result indicates that it is important to determine *which* aspects of turbulent flow (velocity gradients or accelerations) cause damage to or stimulate reactions by plankters before determining the consequences of different flow regimes to these organisms. Since the fraction of time affected falls off much more quickly with increasing thresholds in $\partial u/\partial z$ than it does with increasing thresholds in acceleration for sensitive larvae (i.e., those affected more than 10 % of the time), there may be advantages and disadvantages to reacting to one of these signals versus the other. For example, reacting to accelerations provides robustness of behaviors against small variations in thresholds among individuals or for an individual over time. However, reacting to velocity gradients allows organisms to quickly change how they travel in the flow environment by making only a small change in reaction threshold (e.g., based on developmental stage). As expected, longer reaction times (t_{react}) cause larvae to miss the many transitory fluctuations experienced in realistic flow, so measurement of reaction times may be important to understanding the flow regimes that cause various species of larvae to respond and thus the environments in which they are induced to settle. We also find that larval buoyancy does alter their trajectories, as other models of density effects on the transport of small bodies across vortices also predict (e.g., Crimaldi and Zimmer 2014), yet buoyancy has little effect on the percent of time that larvae spent affected by the two flow fields we analyzed.

While we focus on flow that mimics the turbulent, oscillatory water motion near well-developed fouling communities, it would be interesting to extend this work to realistic flow characteristic of other marine habitats. For instance, our results could be compared to the temporal patterns of accelerations and velocity gradients measured for larval trajectories near fouling communities of different roughness, or near other types of benthic communities (e.g., coral reefs) exposed to bigger waves or more rapid currents. In addition, similar analyses for the trajectories of small organisms in both harbors and the open ocean in calm versus stormy weather would further help us understand what fluid forces zooplankton experience in the ocean and how the variation in these forces might provide information to a zooplankter about its location.

Additionally, although our focus was on the settlement of microscopic larvae into benthic communities, our results also apply to other ecologically important processes such as the transport of zooplanktonic prey to benthic predators (Robinson et al. 2013), the dispersal of gametes, spores, or larvae released by benthic organisms (Thomas 1994;

Szmant and Meadows 2006; Crimaldi and Zimmer 2014), and the transport and mating interactions of demersal zooplankton (Sutherland et al. 2011).

Technical lessons

We found that PIV resolution has a strong effect on the velocity fields we measured, as has been seen for other flow fields, both measured (Lavoie et al. 2007; Worth et al. 2010; Buxton et al. 2011) and simulated (Antonia and Mi 1993; Antonia et al. 1994; Donzis et al. 2008). In addition, we found that velocity gradients in our realistic flows are much more sensitive to PIV resolution than are the velocities, as had been shown in earlier studies of more idealized flow (Donzis et al. 2008). While our medium- and fine-resolution PIV is sufficiently well resolved to measure velocities and accelerations, our medium resolution is not sufficient to accurately measure velocity gradients. Since trajectories of larvae are calculated from the velocity field, we find that our medium and fine resolutions are sufficient to accurately determine larval trajectories.

We found that the spatial resolution of PIV measurements also has a strong effect on the temporal pattern of velocity gradients that the simulated larvae experience. At higher resolution, the velocity gradients experienced by a larva fluctuate more rapidly in time and reach higher magnitudes than they do when calculated using PIV data at lower resolution. The net result is that simulated larvae spend a greater amount of time in large velocity gradients and thus spend a greater fraction of their time affected by the flow if our calculations are done using high-resolution PIV data than if done using low-resolution data. This is true at all thresholds, but becomes most apparent if the threshold is high (i.e., larvae are only affected by very large velocity gradients that occur infrequently).

Caution should be taken when using flow fields measured from PIV to determine the temporal patterns of velocity gradients experienced by microorganisms in flow, or to determine the rotation rates of such organisms. Even our best-resolved flow field of ~η, which is within the typically recommended spatial resolution regime of less than 3η (Antonia and Mi 1993; Antonia et al. 1994), may be to be too coarse. This indicates that experimenters interested in accurately capturing velocity gradients or vorticity for organisms smaller than the Kolmogorov length should probably aim for $\Delta x = 0.5\eta$, a resolution shown to have good overlap of the probability density functions (PDFs) of velocity gradients in idealized turbulent flow (Donzis et al. 2008). Future studies could confirm this recommendation by using our method in a flow field with even higher resolution than we attempted with our experimental setup (ideally at least 0.25η), which would require a field of view that is much smaller than the one employed in our experiments. Unfortunately, there is a trade-off between using high spatial resolution and using a field of view that is large enough to capture large structures in the flow and to follow long trajectories of larvae or particles. Arrays of synchronized cameras could be used to measure flow over larger areas at high resolution, but PIV at such high spatial resolution may also suffer from error due to noise (Saarenrinne and Piirto 2000; Tanaka and Eaton 2007). Thus, it could be a productive avenue of future study to explore simulated larval trajectories in flows computed using direct numerical simulation of the Navier–Stokes equation (DNS) at high resolution, and to find models to connect under-resolved Eulerian PIV flow fields to accurate Lagrangian temporal patterns of velocity gradients. Calculations that use models to determine the time series of velocity gradients along Lagrangian trajectories (summarized in Meneveau 2011) may prove useful in understanding and generalizing the temporal patterns of velocity gradients along trajectories and could be a good complement to the experimental approach used here.

Since the behavioral responses of larvae exposed to very brief and rare encounters with high velocity gradients are not yet known, it is unclear whether the calculated differences in fraction of time affected for larvae simulated in the three flow resolutions is important for the fate of these larvae. Therefore, another interesting direction for future study is to couple the velocity gradients to larval behavior, both by simulating swimming organisms that rotate according to the measured instantaneous vorticity of the flow, and by coupling the larvae reaction above some threshold in velocity gradient or acceleration to a behavior that alters their trajectory, such as cessation of swimming.

In contrast to our results for velocity gradients, we find that the temporal pattern of accelerations that larvae experience along their trajectories does not change significantly within the range of PIV resolutions we used. The near overlap of the PDFs for velocity (Fig. 5) and the close match of average velocities shown in Table 1 between measurements taken at fine and medium resolution show that our medium resolution (2η for lower energy wave and 6η for higher energy wave) is sufficient for measuring velocities and trajectories. Providing the organism does not react to velocity gradients, and accurate rotations of the organism in flow are not needed, resolution can be quite coarse for accurate measurements of trajectories and accelerations.

Organisms larger than the Kolmogorov length can average the flow field over their body size. Therefore, to measure flow fields that accurately capture trajectories of and flow signals experienced by larger organisms, the spacing between vectors can be much larger. For such cases, the spacing between flow velocity vectors needs to be only half of the length of the shortest axis of the organism (e.g., diameter for a spherical or cylindrical organism) so that

spatial derivatives taken by central differencing average over this size.

Acknowledgments We are grateful to B. Nedved, L. Perotti, and M. Shipley for help with the fieldwork, and to T. Cooper for technical assistance with the wave tank experiments and particle image velocimetry analysis. Wave tank studies were conducted at the Kewalo Marine Laboratory, University of Hawaii, and we thank M. Hadfield and his research group for logistical support and useful discussions. This research was supported by National Science Foundation grant Integrative Organismal Systems 0842685 (to MK), and the Miller Institute for Basic Research in Science (fellowship to RP).

References

Abelson A, Denny M (1997) Settlement of marine organisms in flow. Annu Rev Ecol Syst 28:317–339

Antonia RA, Mi J (1993) Corrections for velocity and temperature derivatives in turbulent flows. Exp Fluids 14:203–208

Antonia RA, Zhu Y, Kim J (1993) On the measurement of lateral velocity derivatives in turbulent flows. Exp Fluids 15:65–69

Antonia RA, Zhu Y, Kim J (1994) Corrections for spatial velocity derivatives in a turbulent shear flow. Exp Fluids 16:411–413

Biewener AA, Full RJ (1992) Force platform and kinematic analysis. In: Biewener AA (ed) Biomechanics: structures and systems: a practical approach, Oxford University Press, New York, pp 45–73

Bram JB, Page HM, Dugan JE (2005) Spatial and temporal variability in early successional patterns of an invertebrate assemblage at an offshore oil platform. J Exp Mar Biol Ecol 317:223–237

Bretherton FP (1962) The motion of rigid particles in a shear flow at low Reynolds number. J Fluid Mech 14(2):284–304

Butman CA, Grassle JP, Buskey EJ (1988) Horizontal swimming and gravitational sinking of *Capitella* sp. I (Annelida: Polychaeta) larvae: implications for settlement. Ophelia 29:43–57

Buxton ORH, Laizet S, Ganapathisubramani B (2011) The effects of resolution and noise on kinematic features of fine-scale turbulence. Exp Fluids 51(5):1417–1437

Chan KYK (2012) Biomechanics of larval morphology affect swimming: insights from the sand dollars *Dendraster excentricus*. Integr Comp Biol 52:458–469

Chia F-S, Buckland-Nicks J, Young CM (1984) Locomotion of marine invertebrate larvae: a review. Can J Zool 62:1205–1222

Clay TW, Grünbaum D (2010) Morphology-flow interactions lead to stage-selective vertical transport of larval sand dollars in shear flow. J Exp Biol 213:1281–1292

Clay TW, Grünbaum D (2011) Swimming performance as a constraint on larval morphology in plutei. Mar Ecol Prog Ser 423:185–196

Crimaldi JP, Zimmer RK (2014) The physics of broadcast spawning in benthic invertebrates. Annu Rev Mar Sci 6:141–165

Crisp DJ (1955) The behaviour of barnacle cyprids in relation to water movement over a surface. J Exp Biol 32:569–590

Davidson PA (2004) Turbulence: an introduction for scientists and engineers. Oxford University Press, USA

De Jong J, Cao L, Woodward SH et al (2008) Dissipation rate estimation from PIV in zero-mean isotropic turbulence. Exp Fluids 46:499–515

Denny MW, Nelson EK, Mead KS (2002) Revised estimates of the effects of turbulence on fertilization in the purple sea urchin, *Strongylocentrotus purpuratus*. Biol Bull 203:275–277

Donzis DA, Yeung PK, Sreenivasan KR (2008) Dissipation and enstrophy in isotropic turbulence: resolution effects and scaling in direct numerical simulations. Phys Fluids 20:045108–1–045108–16

Durham WM, Kessler JO, Stocker R (2009) Disruption of vertical motility by shear triggers formation of thin phytoplankton layers. Science 323:1067–1070

Finelli CM, Wethey DS (2003) Behavior of oyster (*Crassostrea virginica*) larvae in flume boundary layer flows. Mar Biol 143:703–711

Fuchs HL, Mullineaux LS, Solow AR (2004) Sinking behavior of gastropod larvae (*Ilyanassa obsoleta*) in turbulence. Limnol Oceanogr 49:1937–1948

Fuchs HL, Hunter EJ, Schmitt EL, Guazzo RA (2013) Active downward propulsion by oyster larvae in turbulence. J Exp Biol 216:1458–1469

Fuchs HL, Gerbi GP, Hunter EJ et al (2015) Hydrodynamic sensing and behavior by oyster larvae in turbulence and waves. J Exp Biol 218:1419–1432

Gaylord B, Hodin J, Ferner MC (2013) Turbulent shear spurs settlement in larval sea urchins. Proc Natl Acad Sci 110:6901–6906

Greene JK, Grizzle RE (2007) Successional development of fouling communities on open ocean aquaculture fish cages in the western Gulf of Maine, USA. Aquaculture 262:289–301

Gross TF, Werner FE, Eckman JE (1992) Numerical modeling of larval settlement in turbulent bottom boundary layers. J Mar Res 50:611–642

Grunbaum D, Strathmann RR (2003) Form, performance and tradeoffs in swimming and stability of armed larvae. J Mar Res 61:659–691

Hadfield MG, Koehl MAR (2004) Rapid behavioral responses of an invertebrate larva to dissolved settlement cue. Biol Bull 207:28–43

Holm ER, Nedved BT, Phillips N et al (2000) Temporal and spatial variation in the fouling of silicone coatings in Pearl Harbor, Hawaii. Biofouling 15:95–107

Hunter T (1988) Mechanical design of hydroids: flexibility, flow forces, and feeding in Obelia longissima. University of California, Berkeley

Jeffery GB (1922) The motion of ellipsoidal particles immersed in a viscous fluid. Proc Royal Soc Lond A 102:161–179

Jimenez J (1997) Oceanic turbulence at millimeter scales. Sci Mar 61:47–56

Jonsson PR, Andre C, Lindegarth M (1991) Swimming behavior of marine bivalve larvae in a flume boundary-layer flow—evidence for near-bottom confinement. Mar Ecol Prog Ser 79:67–76

Karp-Boss L, Jumars PA (1998) Motion of diatom chains in steady shear flow. Limnol Oceanogr 43:1767–1773

Karp-Boss L, Boss E, Jumars PA (2000) Motion of dinoflagellates in a simple shear flow. Limnol Oceanogr 45:1594–1602

Koehl MRA (2007) Mini review: hydrodynamics of larval settlement into fouling communities. Biofouling 23:357–368

Koehl MAR, Cooper T (2015) Swimming in a turbulent world. Integr Comp Biol 55(4):683–697

Koehl MAR, Strother JA, Reidenbach MA et al (2007) Individual-based model of larval transport to coral reefs in turbulent, wave-driven flow: behavioral responses to dissolved settlement inducer. Mar Ecol Prog Ser 335:1–18

Koehl MAR, Crimaldi JP, Dombroski DE (2013) Wind chop and ship wakes determine hydrodynamic stresses on larvae settling on different microhabitats in fouling communities. Mar Ecol Prog Ser 479:47–62

Lavoie P, Avallone G, Gregorio F et al (2007) Spatial resolution of PIV for the measurement of turbulence. Exp Fluids 43:39–51

Mathews JH, Fink KD (1999) Numerical methods using MATLAB. Prentice Hall, Upper Saddle River, NJ

Maxey MR, Riley JJ (1983) Equation of motion for a small rigid sphere in a nonuniform flow. Phys Fluids 26:883–889

McDonald KA (2012) Earliest ciliary swimming effects vertical transport of planktonic embryos in turbulence and shear flow. J Exp Biol 215:141–151

McEdward LR (1995) Ecology of marine invertebrate larvae. CRC Press, Boca Raton

Mead KS, Denny MW (1995) The effects of hydrodynamic shear stress on fertilization and early development of the purple sea urchin *Strongylocentrotus purpuratus*. Biol Bull 188:46–56

Meneveau C (2011) Lagrangian dynamics and models of the velocity gradient tensor in turbulent flows. Annu Rev Fluid Mech 43:219–245

Nowell ARM, Jumars PA (1984) Flow environments of aquatic benthos. Annu Rev Ecol Syst 15:303–328

Okamura B (1984) The effects of ambient flow velocity, colony size, and upstream colonies on the feeding success of bryozoa. I. Bugula stolonifera Ryland, an arborescent species. J Exp Mar Biol Ecol 83:179–193

Peters F, Marrasé C (2000) Effects of turbulence on plankton: an overview of experimental evidence and some theoretical considerations. Mar Ecol Prog Ser 205:291–306

Pope SB (2000) Turbulent flows, 1st edn. Cambridge University Press, Cambridge

Rabiner LR, Gold B (1975) Theory and application of digital signal processing. Prentice-Hall, Englewood Cliffs, NJ

Raffel M, Willert CE, Kompenhans J (1998) Particle image velocimetry: a practical guide. Springer, Berlin

Raupach MR, Antonia RA, Rajagopalan S (1991) Rough-wall turbulent boundary layers. Appl Mech Rev 44:1–25

Robinson H, Finelli CM, Buskey EJ (2007) The turbulent life of copepods: effects of water flow over a coral reef on their ability to detect and evade predators. Mar Ecol Prog Ser 349:171–181

Robinson HE, Finelli CM, Koehl MAR (2013) Interactions between benthic predators and zooplanktonic prey are affected by turbulent Waves. Integr Comp Biol 53:810–820

Saarenrinne P, Piirto M (2000) Turbulent kinetic energy dissipation rate estimation from PIV velocity vector fields. Exp Fluids 29:S300–S307

Schabes M (1992) Mechanical consequences of the association between the solitary ascidian, *Styela clava* Herdman, 1881, and its epibiota. M.S. Thesis, University of California, Berkeley

Strathmann RR, Grunbaum D (2006) Good eaters, poor swimmers: compromises in larval form. Integr Comp Biol 46:312–322

Sutherland JP, Karlson RH (1977) Development and stability of the fouling community at Beaufort, North Carolina. Ecol Monogr 47:425–446

Sutherland KR, Dabiri JO, Koehl MAR (2011) Simultaneous field measurements of ostracod swimming behavior and background flow. Limnol Oceanogr Fluids Environ 1:135–146

Szmant AM, Meadows MG (2006) Developmental changes in coral larval buoyancy and vertical swimming behavior: implications for dispersal and connectivity. In: Proceedings of 10th international coral reef Symposium, pp 431–437

Tanaka T, Eaton JK (2007) A correction method for measuring turbulence kinetic energy dissipation rate by PIV. Exp Fluids 42:893–902

Thomas F (1994) Physical properties of gametes in three sea urchin species. J Exp Biol 194:263–284

Thomas WH, Gibson CH (1990) Effects of small-scale turbulence on microalgae. J Appl Phycol 2:71–77

Thorpe SA (2007) An introduction to ocean turbulence. Cambridge University Press, Cambridge

Toschi F, Bodenschatz E (2009) Lagrangian properties of particles in turbulence. Annu Rev Fluid Mech 41:375–404

Townsend AA (1980) The structure of turbulent shear flow. Cambridge University Press, Cambridge

Variano EA, Cowen EA (2008) A random-jet-stirred turbulence tank. J Fluid Mech 604:1–32

Vogel S (2013) Comparative biomechanics: life's physical world, 2nd edn. Princeton University Press, Princeton

Welch P (1967) The use of fast Fourier transform for the estimation of power spectra: a method based on time averaging over short, modified periodograms. IEEE Trans Audio Electroacoust 15:70–73

Wheeler JD, Helfrich KR, Anderson EJ et al (2013) Upward swimming of competent oyster larvae *Crassostrea virginica* persists in highly turbulent flow as detected by PIV flow subtraction. Mar Ecol Prog Ser 488:171–185

Wheeler JD, Helfrich KR, Anderson EJ, Mullineaux LS (2015) Isolating the hydrodynamic triggers of the dive response in eastern oyster larvae. Limnol Oceanogr 60(4):1332

Worth NA, Nickels TB, Swaminathan N (2010) A tomographic PIV resolution study based on homogeneous isotropic turbulence DNS data. Exp Fluids 49:637–656

Yeung P (2002) Lagrangian investigations of turbulence. Annu Rev Fluid Mech 34:115–142